

# XXResolution Correspondence Networks

Georgi Tinchev\*  
 Oxford Robotics Institute  
 University of Oxford  
 gtinchev@robots.ox.ac.uk

David Mitchell  
 XYZ Reality  
 david.mitchell@xyzreality.com

Shuda Li  
 XYZ Reality  
 shuda.li@xyzreality.com

Kai Han  
 Visual Geometry Group  
 University of Oxford  
 khan@robots.ox.ac.uk

Rigas Kouskouridas  
 XYZ Reality  
 rigas.kousk@xyzreality.com

<https://xyz-r-d.github.io/xrcnet>

## Abstract

*In this paper, we aim at establishing accurate dense correspondences between a pair of images with overlapping field of view under challenging illumination variation, viewpoint changes, and style differences. Through an extensive ablation study of the state-of-the-art correspondence networks, we surprisingly discovered that the widely adopted 4D correlation tensor and its related learning and processing modules could be de-parameterised and removed from training with merely a minor impact over the final matching accuracy. Disabling these computational expensive modules dramatically speeds up the training procedure and allows to use 4 times bigger batch size, which in turn compensates for the accuracy drop. Together with a multi-GPU inference stage, our method facilitates the systematic investigation of the relationship between matching accuracy and up-sampling resolution of the native testing images from 1280 to 4K. This leads to discovery of the existence of an optimal resolution  $\mathbb{X}$  that produces accurate matching performance surpassing the state-of-the-art methods particularly over the lower error band on public benchmarks for the proposed network.*

## 1. Introduction

Establishing dense image correspondences is a fundamental problem for many computer vision applications, from Structure-from-Motion (SfM) [41, 43], visual Simultaneous Localisation and Mapping (SLAM) [23] to image retrieval [51], image style transfer [49], and scene understanding [22]. Traditionally, point correspondences between a pair of images are found through a sparse detection-

description and matching pipeline. Particularly, a key point detector [37, 12] is first used to collect a set of sparse interest points from input images while a feature descriptor [27, 2, 20] extracts a unique description of a local image patch centred at the detected key point location. In the end, the point correspondences between the query image and the reference one are calculated by searching the candidate matching pairs for small descriptor distances or using the ratio test between the best and the second best matches [27].

In the last few years we have witnessed a dramatic improvement over all stages of the sparse correspondence pipeline mostly using machine learning [8, 9, 34, 46, 34]. In addition to the feature detectors and descriptors, the matching stage has also been extensively studied and new algorithms taking into account both inter-image and intra-image constraints make the matching stage more reliable than before [38, 28, 46, 54]. However, sparse correspondence methods are not straightforward to be adapted to produce per pixel matches which are often required for image warping, style transfer, or dense 3D reconstruction. A naive extension from sparse methods, for example, is to densely extract feature descriptors and use brute force matching. However, this is prohibitively expensive for high resolution images. Furthermore, to achieve the best performance, the detection-description and matching pipeline typically requires each stage to be trained separately, which introduces extra difficulties when being deployed to new sensory data. For example, the top performer on the visual localisation benchmark [55] combines the SuperPoint (SP) [8] and SuperGlue (SG) [38] and the SP detector-descriptor has to be trained separately with SG.

In contrast, the dense correspondence methods [26] and particularly Deep Correspondence Networks (DCN) [7, 31,

\*Work done while on internship with XYZ Reality.



Figure 1: XRCNet highlights: **Left tuple**: Using high resolution feature maps allows XRCNet to accurately pinpoint the target key point location given a query point in the source image. Note that the image contains challenging repetitive patterns of the letter 'a' that confuse the network when using a low resolution image (left most). **Right**: XRCNet without using any geometric constraints is capable of producing state-of-the-art matching accuracy and reliably match under extreme illumination and style differences (best viewed in PDF with zoom).

53, 49, 36, 35] that emerged in recent years, represent a highly competitive alternative for their capability of producing good quality per pixel correspondences. DCNs also unify the detection-description and matching pipeline into one single architecture using standard feature backbones such that it can be trained end-to-end. Moreover, DCNs are shown to be able to quickly adapt to images of high resolution or larger feature maps while being deployed into consumer products [36, 35, 23, 49, 13].

In this paper, we present a novel dense correspondence methodology that is capable of processing high resolution images and produce reliable and highly accurate matching results as shown in Fig. 1. More importantly, light-weight correspondence networks allows us to investigate an intriguing questions for all DCNs: The widely adopted testing protocol of up-sampling the testing images seems always beneficial for improving matching accuracy. up-sampling the testing image always lead to higher accuracy? If not, Does it exist an optimal resolution  $\mathbb{X}$  given testing images in a dataset? In this work, we introduce XResolution Correspondence Network (XRCNet), a light-weight architecture designed to answer these questions while achieving state-of-the-art performance.

Our work is directly inspired by the recently introduced strategy of using extensive ablation studies to either achieve more accurate visual representations [4] or highly impactful training procedures or architecture refinements that improve model accuracy [16]. Approaching the dense correspondence problem with the same strategy, we start by carrying out extensive ablation studies with various training configurations over the state-of-the-art dense correspondence networks and made several key observations. First, the widely adopted 4D correlation tensor and its related filtering modules [36, 35, 49, 13] can be de-parameterised and even removed from the training stage at the cost of a

small drop in accuracy. Second, switching to a much shallower feature backbone also has limited impact to the overall matching results. Third, the combination of the first two discoveries results in the light-weight XRCNet. During the training stage, XRCNet enjoys a significantly smaller memory footprint and much faster speed than the state-of-the-art methods (see Tab. 1). This allows us to use 4 times larger batch size and increase the number of epochs within roughly the same amount of training time using the same hardware. The latter compensates for the slight deterioration of the accuracy levels. When combined with a multi-GPU inference method, it allows us to evaluate the matching accuracy of XRCNet using image size up to 4K, by which we discover the existence of an optimal up-sampling resolution for XRCNet to achieve the best accuracy. Interestingly, increasing the resolution is not always beneficial possibly because the relative size of the receptive field to the image might decrease, which then renders the network prediction less accurate. Overall, the contributions of the paper can be summarised as follow:

- We carried out extensive tests and a thorough ablation study over the state-of-the-art DCNs and made several key observations that lead to the introduction of a simple and light-weight multi-resolution neural network architecture named as the XResolution Network (XRCNet).
- XRCNet is capable of training with much larger batch size and faster per image learning speed. During inference, XRCNet can take in images with higher resolution than most of the previous work and allows us to search for the optimal resolution  $\mathbb{X}$  to up-sample the testing image for a correspondence task.
- XRCNet achieves state-of-the-art accuracy on two challenging datasets — HPatches [1] and InLoc [44],

while performing competitively on Aachen Day-Night [39, 40].

## 2. Related work

As the correspondence algorithm is a basic building block in computer vision, there is a huge volume of related works that can be found in the literature. Existing methods range from sparse to dense correspondence estimation. Sparse correspondence algorithms typically adopt the three-stage pipeline of detection-description and matching. Each stage has received extensive research focus over the last two decades. For key point detection and description, handcrafted methods SIFT, SURF, BRIEF [27, 2, 3] and their variants [20, 42] were introduced for first detecting, then describing and finally matching a sparse set of key points. Taking into account the local region around each key point, a feature vector of floating points or binary numbers can be extracted to uniquely represent the key points for feature matching or scene description [10]. Most of the modern descriptors [45, 52, 9, 46, 34, 28] focus on data-driven learning approaches, while evaluating the matching performance of descriptors is performed either by measuring the distances between a pair of descriptors or through the ratio test [27]. Modern matching approaches take into account the constraints between feature descriptors to enhance the matching success rate [54, 38]. Particularly, SuperGlue [38] represents the state-of-the-art matching success rate against efficiency by exploring the inter/intra-image information.

Sparse correspondence algorithms achieve efficiency by attending to a small set of salient points in the images, however, for applications such as SfM [41, 43], style transfer [49] or view synthesis [33] where per-pixel correspondence maps are often required, simply scaling up the sparse approach becomes prohibitively expensive. In contrast, dense correspondence approaches focus on bridging this gap. One of the earliest dense methods [26] uses dense feature descriptors and regularising within the local region to achieve a consistent dense flow field. In recent years, deep semantic correspondence networks [14, 19, 36, 29, 17, 22] have demonstrated the potential of densely associating key points between a pair of input images. However, as these approaches focus on matching high level regions, they either require a large number of feature channels, typically larger than 1024 [19, 29, 30], or build on top of the 4D correlation tensor and expensive 4D filtering [36, 17, 22]. This fact makes it very difficult to scale up to higher image resolutions, which is critical for accurate data association [36, 35, 23]. SparseNC overcomes the scalability problem by projecting the memory consuming 4D correlation tensor into a sub-manifold and uses the Minkowski convolution [6] to approximate the 4D filtering, however the approximation reduces the performance of the network. Du-

alRC [23] keeps the original 4D correlation tensor in its original space, but relies on a coarse to fine re-weighting mechanism to guide the search in a fine resolution correlation map for the best match. In this work, we further reduce the network redundancy by limiting the operation of the 4D correlation tensor. Combined with a much shallower feature backbone, our proposed approach can process images with higher resolution than all previous dense networks on the same hardware setup.

Establishing dense correspondences is also relevant to stereo networks [48], deep visual odometry [50] and optical flow networks [48] since these algorithms involve calculating a dense flow field that associates two individual images. However, a stereo architecture typically assumes that the input views are rectified and the images are captured under roughly the same illumination environment, while the viewpoints are relatively close to each other, which can be viewed as a simplified version of the correspondence problem. Similarly, both the tasks of optical flow estimation and visual odometry are considered to be much more constrained than the general correspondence problem, since both assume that the viewpoints of the input images are close both temporally and spatially in terms of the 6D manifold of the camera poses.

## 3. Methodology

In this work we present a new dense correspondence methodology working with input images of higher resolution than any other state-of-the-art dense method and attaining higher accuracy particularly for small error bands. In this section, we first describe the DCN framework illustrated in Fig. 2, then the redundant module is ablated to form the  $\mathbb{X}$ RCNet.

Given a pair of images  $\mathbf{I}$  and  $\mathbf{I}'$ , we want to estimate a per-pixel correspondence map that associates a 2D key point from the source image  $(x, y) \in \mathbf{I}$  to a point in the target image  $(x', y') \in \mathbf{I}'$ . To reliably associate the point, we first adopt a standard multi-level feature backbone  $\mathbf{F} = f(\mathbf{I}; \theta_0)$ , where  $\theta_0$  are learnable variables. Particularly,  $\mathbf{F} = \{\mathbf{F}_f, \mathbf{F}_c\}$  where  $\mathbf{F}_f \subset \mathbb{R}^{C \times \Omega_f}$  is one layer of the feature map within a 2D domain  $\Omega_f$  and  $\mathbf{F}_c \subset \mathbb{R}^{C \times \Omega_c}$  is another layer of the feature map within  $\Omega_c$ . Subscripts  $f$  and  $c$  represent the fine and coarse resolutions, while  $C$  stands for the number of feature channels. Previous works [36, 35, 49, 23] make use of a 4D correlation tensor  $\mathbf{C} \subset \mathbb{R}^{\Omega \times \Omega'}$ , where  $\mathbf{C}_{(x,y,x',y')} = \mathbf{F}(x, y)^\top \mathbf{F}'(x', y')$ . Note that all values in the feature maps are positive due to the ReLU activation layer in the feature backbone  $f(\cdot)$  immediately before calculating the correlation. The features are typically normalised along the channels —  $\|\mathbf{F}(x, y)\|_2 \triangleq 1$  and thus the dot product of two feature vectors is within the range  $[0, 1]$ . The 4D correlation tensor represents all possible candidate matching pairs from the source to the target image.

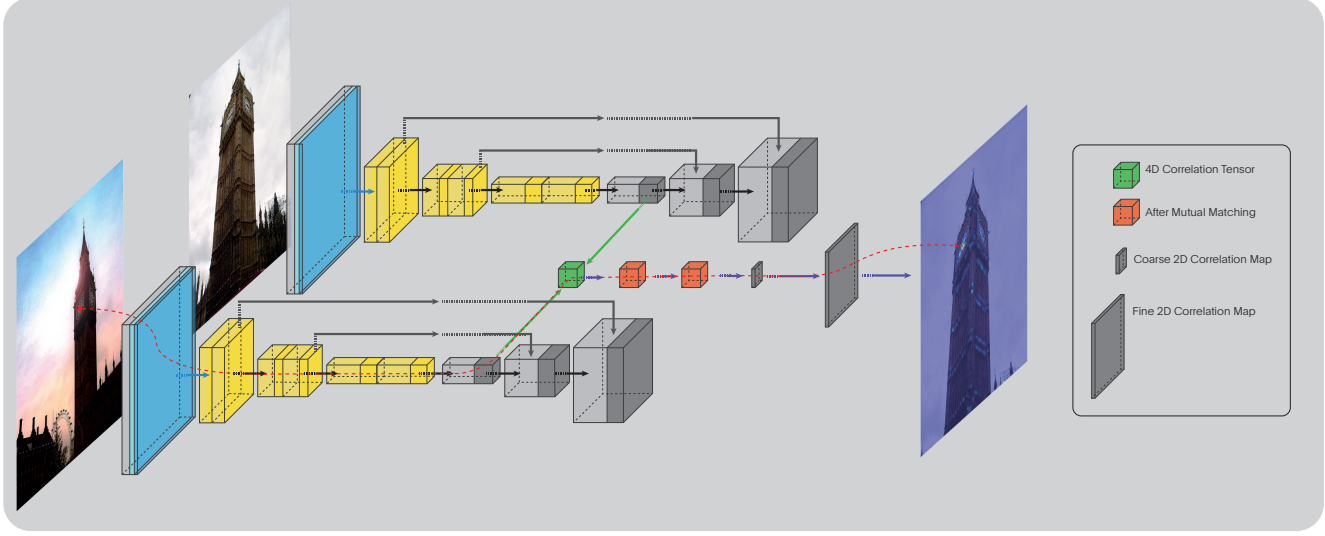


Figure 2: The architecture of XRCNet. The deep correspondence neural network takes a Siamese-like structure. Each branch is composed of a feature encoder (gray and yellow from the left) and FPN-like decoder (the gray blocks to the right). From the coarse layer of FPN, a 4D correlation tensor is calculated (green) and filtered by the mutual matching (MM) layer to get the filtered 4D tensor (orange). After that the tensor is filtered again by the MM layer. Given a query key point from the source image (bottom left), the corresponding features are selected from the FPN coarse layers and query into the 4D tensor.

### 3.1. Neighbourhood consensus

Initially introduced in NCNet [36], a set of 4D convolutions with learnable variables is trained to filter the noise from the raw correlation tensor. The local 4D volume contains all possible matching pairs within the neighbourhood of the source and target image from which a filtering process is employed in order to collect consensus from them. Neighbourhood Consensus (NC) filtering can be formulated as  $\hat{\mathbf{C}} = N(\mathbf{C}; \theta_1) + N(\mathbf{C}^\top; \theta_1)^\top$  where  $N(\cdot)$  represents the NC filtering consisting of a sequence of 4D convolution layers.  $\mathbf{C}^\top$  is the permutation operation such that  $\mathbf{C}_{(x,y,x',y')} = \mathbf{C}_{(x',y',x,y)}^\top$  and  $\theta_1$  are the learnable parameters in the NC filtering. The first term corresponds to the matching direction from source to the target and the second term from target to the source. Since the matching direction is independent of the filter weights,  $\theta_1$  is shared by the two filtering stages. The result  $\hat{\mathbf{C}}$  has the same dimensionality as  $\mathbf{C}$  that contains the filtered correlation scores.

To improve accuracy soft Mutual Matching (MM) filtering layers can also be applied before and after the NC filtering to dynamically adjust the scale of the correlation tensor:

$$\mathbf{M}_{(x,y,x',y')} = \frac{\mathbf{C}_{(x,y,x',y')}}{\max_{\forall (x',y') \in \Omega'} \mathbf{C}_{(x,y,x',y')} + \epsilon} \quad (1)$$

$$\mathbf{M}'_{(x,y,x',y')} = \frac{\mathbf{C}_{(x,y,x',y')}}{\max_{\forall (x,y) \in \Omega} \mathbf{C}_{(x,y,x',y')} + \epsilon} \quad (2)$$

$$\hat{\mathbf{C}}_{(x,y,x',y')} = \mathbf{M}_{(x,y,x',y')} \mathbf{C}_{(x,y,x',y')} \mathbf{M}'_{(x,y,x',y')} \quad (3)$$

where  $\epsilon$  is a infinite small value to improve the numerical stability and prevent errors during the degenerating scenario

that the maximum correlation in a domain is 0. It can be seen that the MM layer contains no learnable parameters. As shown in equations 1 and 2 the MM layer first converts the correlation scores into probabilities by normalising using the maximum correlations with respect to the target domain  $\Omega'$  and source domain  $\Omega$ , respectively. The multiplication of  $\mathbf{M}_{(x,y,x',y')}$  and  $\mathbf{M}'_{(x,y,x',y')}$  can be viewed as the joint probability of matching from source to target and from target to source providing the matching along both directions are independent. Ablating MM layer reduces matching accuracy possibly because the MM layer adjusts the scores in the correlation tensor. More detailed discussion will be provided in Section 3.3.

In the end, given a query point  $(x, y) \in \mathbf{I}$ , the best matches can be found at  $(\hat{x}', \hat{y}') = \arg \max_{\forall (x', y') \in \Omega'} \hat{\mathbf{C}}_{(x,y,x',y')}$ . The dense correspondence map can be established by calculating  $(\hat{x}', \hat{y}')$  for every pixel in the source image. In addition, the maximum correlation scores  $\mathbf{S} \subset \mathbb{R}^\Omega$  represent a good indication of the matching reliability, where  $\mathbf{S}(x, y) = \max_{\forall (x', y') \in \Omega'} \hat{\mathbf{C}}_{(x,y,x',y')}$ . A sub-set of top  $k$  reliable matches  $\mathbb{S} = \{\mathbf{S}\}_k$  can be collected accordingly, or alternatively set a threshold to remove unreliable matches [36, 35, 22].

### 3.2. Correlation re-weighting

The main bottleneck for the aforementioned NC filtering and MM layer lies in the fact that the 4D correlation is very expensive to calculate and difficult to scale up. To deal with the problem, SparseNC [35] projects the corre-

Table 1: Ablation study. Training is performed on a single Tesla V100-SXM2 GPU. We use batch size of 16 and Adam optimiser [18] for all configurations. We run the training 15 epochs in total. Strong key point supervision is adopted for all methods. The test image up-sample resolution is 1.6K. The Sum of Area under the curve of MMA represent the overall accuracy over multiple error bands. All approaches are trained using ResNet18.

Component/Method	DualRC	SparseNC	NCNet	$\mathbb{XRC}_1$	$\mathbb{XRC}_2$	$\mathbb{XRC}_3$	$\mathbb{XRC}_4$
4D correlation tensor	✓	✓	✓	✓	✓	✓	✗
NC filtering	✓	✓	✓	✗	✗	✗	✗
Mutual matching	✓	✗	✓	✓	✓	✗	✗
DualRC re-weighting	✓	✗	✗	✓	✗	✓	✓
Memory (GB)	6.78	3.73	5.40	4.57	4.25	4.36	4.21
Training time (s)	2.73	0.49	0.73	0.48	0.26	0.35	0.27
Sum of Area	3.90	3.20	3.61	3.65	2.49	3.36	3.26

lation tensor onto a sub-manifold that contains the top  $k$  highest correlation scores for each source or target pixels. The 4D filtering is then approximated using the Minkowski operation [6]. In this way, the memory footprint can be dramatically reduced. Higher resolution images can fit into the memory leading to improved performance. However, such an approximation affects the accuracy as shown in [23]. Li et al [23] propose to use a hierarchical architecture where the coarse resolution feature map  $\mathbf{F}_c$  is used to calculate the 4D tensor for NC filtering and MM filtering. Then, the 2D correlation map  $\mathbf{C}^c(x, y) \subset \mathbb{R}^{\Omega_c}$  at location  $(x, y) \in \mathbb{R}^{\Omega_c}$  is used to guide the searching for the best matches in the fine feature map by re-weighting the correlation map at the fine resolution  $\mathbf{C}^f(x, y)$ . Specifically,  $\hat{\mathbf{C}}^f(x, y) = U(\mathbf{C}^c(x, y)) \cdot \mathbf{C}^f(x, y)$ , where  $U()$  is a de-parameterised up-sampling function,  $\cdot$  represents the element-wise multiplication, and  $\hat{\mathbf{C}}^f(x, y)$  is the re-weighted correlation map with the fine resolution. More accurate matches can be localised at  $(\hat{x}', \hat{y}')_f = \arg \max_{\forall (x', y') \in \Omega'_f} \hat{\mathbf{C}}^f_{(x, y, x', y')}$ . Note that the correlation re-weighting contains no learnable parameters.

### 3.3. Ablation study and $\mathbb{XRCNet}$

To better understand the pros and cons of the mainstream DCN architectures, we conducted an ablation study over several state-of-the-art methods, namely, NCNet [36], SparseNC [35], and DualRC [23]. The left column in Tab. 1 lists the key modules shared by the DCNs. We tested the performance of all possible combinations of the key modules using the same training protocol on the MegaDepth dataset [24] following the work of [9] - all baselines are trained with strong supervision with ResNet18 with 256 channels and hard relocalization [35] for a fair comparison. The evaluation over feature backbones is discussed in Fig. 7. For each configuration, we record the average memory consumption, training speed, and the overall matching accuracy. The accuracy measurements are the sum of the area below the Mean Matching Accuracy (MMA) curve on

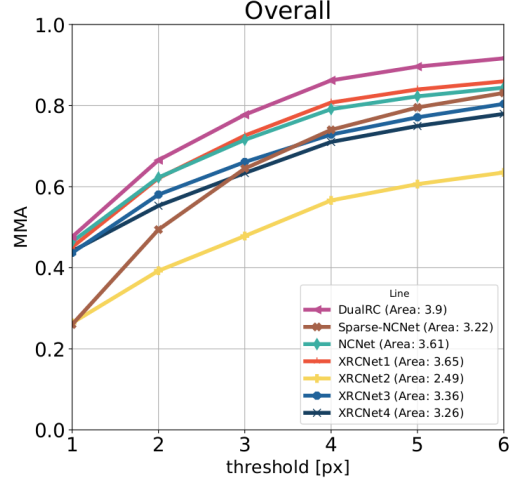


Figure 3: Quantitative evaluation of Neighbourhood Consensus architectures on the HPatches dataset.

the HPatches dataset, comprised of challenging scenes with illumination and viewpoint variation. In addition to Tab. 1, we also plot the accuracy of MMA in Fig. 3 for completeness.

From the experiments, we observe that although all the modules of DCN contribute to the accuracy, they come with a variety of costs. Particularly, 1) the 4D NC filter consumes nearly 50% more memory and is more than 5 times slower comparing DualRC and  $\mathbb{XRC}_1$ . SparseNC reduces the expense of NC filter using the sparse 4D correlation with Minkowski convolution [6] but at the cost of degrading accuracy. 2) The DualRC re-weighting often plays an important role to the accuracy comparing DualRC with NCNet and  $\mathbb{XRC}_1$  with  $\mathbb{XRC}_2$ . 3) Mutual matching layer contributes relative less to accuracy but is also cheap to calculate comparing  $\mathbb{XRC}_1$  with  $\mathbb{XRC}_3$  and therefore we do not remove it. 4) Removing both NC filtering and DualRC re-weight dramatically increases the speed but also decreases the accuracy for  $\mathbb{XRC}_2$  significantly. 5) Removing the 4D correlation tensor, similar to UCN [7], hurts the performance for  $\mathbb{XRC}_4$  compared to  $\mathbb{XRC}_3$ . To summarise, we select  $\mathbb{XRC}_1$  as the default architecture of  $\mathbb{XRCNet}$ , which is about 5 times faster than DualRC but nearly 50% smaller in terms of memory costs. Also, it allows us to adopt 4 times larger batch size during training and can run up to 40 epochs in about same amount of time of training DualRC for 15 epochs. Fig. 1 (left) shows qualitative examples of removing the NC module and the proposed alternative.

The prediction of  $\mathbb{XRCNet}$  is 2D correlation maps as illustrated in Fig. 2. The loss can be then calculated using the F-norm between the prediction and the ground truth distribution [22, 23, 49, 13]. Particularly, we get the ground truth distribution by converting a 2D key point coordinate into a Probability Density Function (PDF). Specifically, we assign the probability of 4 pixels that are the nearest neigh-

bours of the ground truth key point according to their normalised 2D distance. Then the PDF is further filtered by a  $3 \times 3$  Gaussian kernel [22]. To keep the ablation test fair, all the networks in Tab. 1 are supervised using the same loss term.

**XRCNet Inference** We distribute various key modules illustrated in Fig. 2 over multiple GPUs during inference to allow images with much larger resolution to be processed efficiently. Together with the low-cost but relatively accurate XRC<sub>1</sub>, we can address the critical question of how the input image resolution affects the matching accuracy of a DCN. To this end, we evaluate XRC<sub>1</sub> using various image resolutions ranging from 1280 to 4K. More details are provided in section 4.2. The source code for both training and evaluation is attached in the supplementary materials.

## 4. Experiments

In this section, we describe the experiments we conducted to evaluate the performance of XRCNet, the training strategy and we discuss the question of the relationship between the input image resolution and matching accuracy.

**Implementation details** The XRCNet training and evaluation code is implemented using PyTorch [32]. For the feature backbone, we mainly evaluated the ResNet101/50/18 [15], HRNet64/32/18 [47, 5] and the FPN256/128 [25]. The ResNet and HRNet are pre-trained on ImageNet [21] and kept fixed during all training procedures. The parameters of the FPN layers are trained from scratch. The configuration of ResNet101 is adopted from [36], the ResNet18 is truncated after the 3rd layer, the coarse feature map is extracted from the 3rd layer in the ResNet18 and the coarse layer is taken from the output of layer 1. The FPN architecture is identical to the original work of FPN [25] except that a ReLU layer is inserted before the feature normalisation. For HRNet we tested 18, 32, and 64 channels configurations. We truncated HRNet after the third stage in order to keep the input image ratio identical to ResNet. Here we considered both including and excluding the fusing (transition) stages. In addition, we use the output of the first branch as the fine feature map and the output of the third branch as the coarse feature map in order to be consistent to the fine to coarse ratio we used for ResNet. We train our model using the Adam optimiser with an initial learning rate of 0.01 and momentum 0.9. The batch size is 64. The learning rate is halved for every 5 epoch until 15 and remain constant till the 40th epoch. The model with lowest validation error is adopted for the final evaluation. It is worth pointing out that comparing with the training in Tab. 1 which only runs 15 epochs and uses batch size of 16 as previous work, the training with more epochs and a larger batch size result in a much higher accuracy which can be seen by comparing Fig. 6 and the bottom row of Tab. 1.

Table 2: The size statistics of the image size in the 3 testing datasets. The minimum, mean, and maximum size over height and width recorded. HPatches has the lowest mean image resolution and InLoc has the highest resolution.

	HPatches		InLoc		Aachen Day-Night	
	h	w	h	w	h	w
min	380	512	1200	1200	1063	1063
mean	780	980	2397	2531	1268	1498
max	1411	1536	4032	4032	1600	1600

**Training data** We adopt the same training protocol as D2Net [9] on the MegaDepth dataset [24]. MegaDepth includes 196 scenes and the corresponding 3D point clouds created using SfM [41, 43]. The camera internal and external parameters are also jointly estimated and provided by the dataset. We follow the same methodology of [9] to extract a sparse set of ground truth correspondent points. Only image pairs with more than 50% of overlapping field of view are selected as training pairs (15,070). The validation image pairs (14,638) are selected from scenes containing more than 500 good pairs. All training pairs are randomly shuffled to avoid over-fitting to specific scenes.

### 4.1. Correspondence Evaluation

**HPatches** is widely used for evaluating sparse feature matching and dense correspondence algorithms [1]. It contains two main challenges — the viewpoint and illumination variations consisting of 56 and 52 sequences of testing images respectively. Each sequence contains 6 images and the first image is matched against the remaining ones. The native image size is reported in Tab 2. Testing images contain both indoor and outdoor scenes. The ground truth homography is provided so that the correspondences can be densely evaluated. The evaluation procedure is adopted from [9, 34, 35, 23] to allow direct comparison with these baseline methods. The evaluation metric used is the Mean Matching Accuracy (MMA) that estimates the average number of correct matches over the total number of matches using top 2000 proposed matches by the testing neural networks, where the correct matches are defined as the distance between the predicted 2D key points to ground truth. XRCNet sets a new accuracy standard as it can be seen at the comparative evaluation graph shown in Fig. 4.

**Aachen Day-Night** dataset [39, 40] is a challenging outdoor relocalisation dataset. The Day-Night relocalisation challenge contains 98 night query images to be relocalised with respect to 20 day-time candidate images. The performance of XRCNet compared to the baselines on the night query images is shown in Tab. 3, while an example qualitative comparison and the produced 2D heatmap in the reference image are shown in Fig. 8 (right). We provide 3D re-

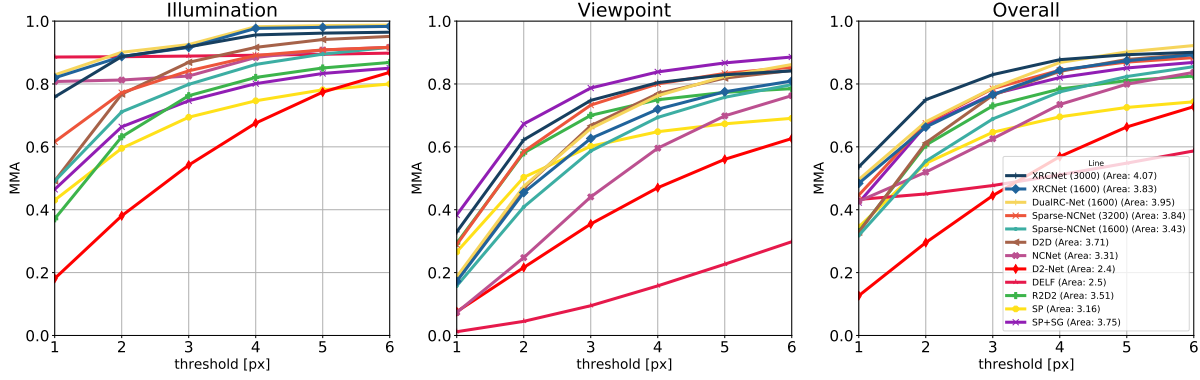


Figure 4: The comparison of XRCNet with the state-of-the-art correspondence networks on the HPatches dataset. It can be seen that XRCNet when using the up-sampled testing images of 3000 surpassed all other methods, i.e. Deep Local Feature Network (DELF) [31], DualRC [23], Sparse-NCNet [35], SP [8], SG [38].

Table 3: Evaluation on the Aachen dataset.

Error Band	ASLFeat+OANet	D2-Net	SparseNC	R2D2	DualRC-Net	SP + SG	XRCNet-1.6k
0.25m & 2°	77.6	74.5	76.5	76.5	79.6	79.6	76.5
0.5m & 5°	89.8	86.7	84.7	90.8	88.8	90.8	85.7
5m & 10°	100.0	100.0	98.0	100.0	100.0	100.0	100.0

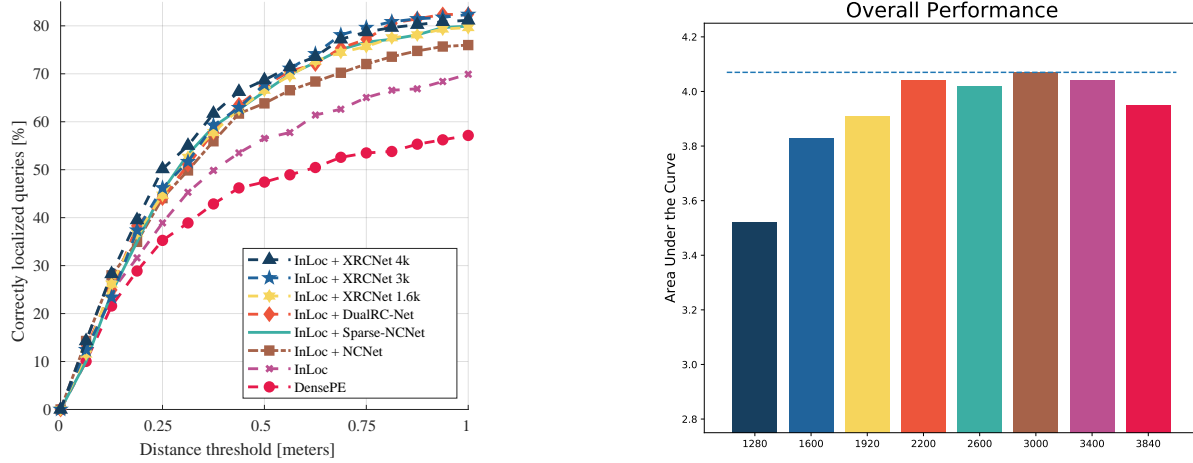


Figure 5: Pose accuracy of InLoc measured by the percentage of correctly localised queries over different distances.

construction results of our XRCNet and DualRC in the supplementary material. XRCNet achieves commensurate performance to the state-of-the-art, while also having a much smaller memory footprint for the used input resolution size and faster inference speed (see Tab. 1).

**InLoc** mainly contains indoor images captured with a different type of sensors [44]. It is a popular benchmark for evaluating the accuracy of camera localisation with respect to large variety of indoor scenes. Reference images are obtained with a 3D scanner and the query images are captured using a mobile phone several months later to introduce extra non-static challenges. InLoc contains significant viewpoint changes and illumination variation. We adopt the evaluation

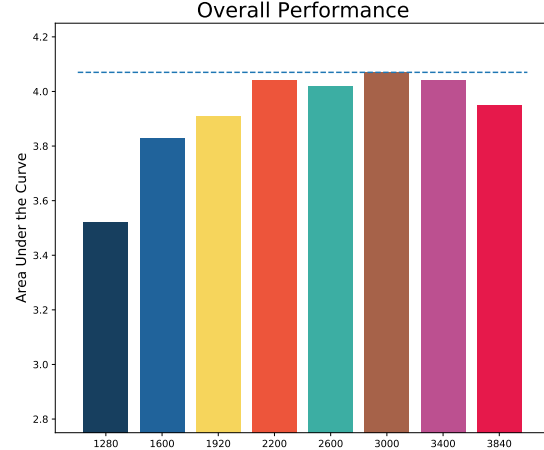


Figure 6: Evaluation of the optimal up-sampling resolution. The height of each bar is the Sum of Area under the curve of the MMA, which represent the overall accuracy. It can be seen that both the low and high up-sampling resolution have a negative impact over the XRCNet's accuracy.

procedure of [44] to find the top 10 candidate database images for each query image. XRCNet is used to calculate the matches between them, and the final 6D camera pose is estimated using PnP [11] and dense pose verification [44]. The results are provide in Fig. 5 and Tab. 4 which show XRCNet significantly outperform the others.

#### 4.2. Optimal Resolution X

A common practice to achieve better accuracy in previous works, is to up-sample the original images to a higher

Table 4: Evaluation on the InLoc dataset. Best result is shown in **bold** and second best is underlined.

Error Band	DualRC	SparseNC	NCNet	InLoc	DensePE	D2-Net	R2D2	$\mathbb{X}$ RCNet-1.6k	$\mathbb{X}$ RCNet-3k	$\mathbb{X}$ RCNet-4k
0.25m & $10^\circ$	44.1	45.6	44.1	38.9	35.3	43.2	<u>47.3</u>	44.7	46.2	<b>50.2</b>
0.5m & $10^\circ$	67.5	66.3	63.8	56.5	47.4	61.1	67.2	66.6	<u>67.8</u>	<b>68.7</b>
1m & $10^\circ$	<b>82.4</b>	79.9	76.0	69.9	57.1	74.2	73.3	79.6	<b>82.4</b>	81.2

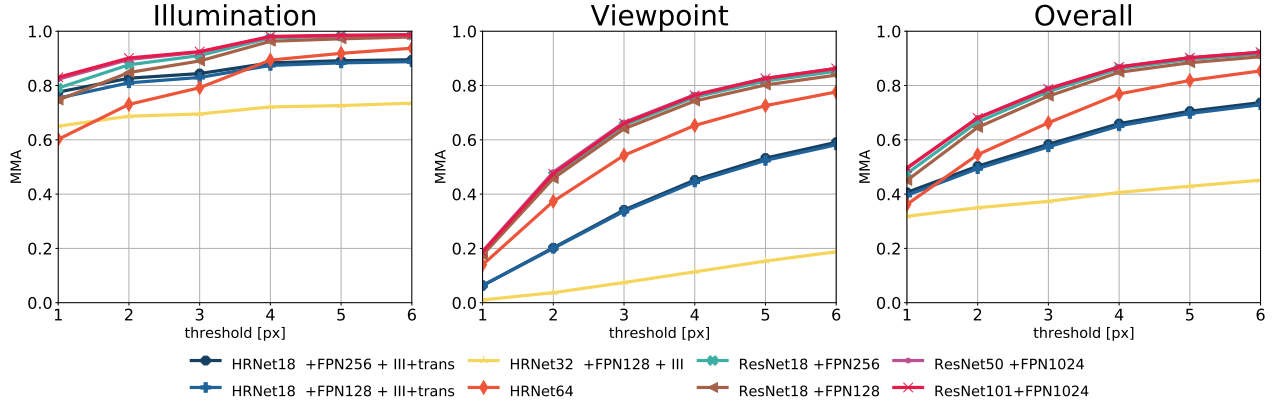


Figure 7: Comparison of different backbone architectures considered for dense correspondence matching.

resolution that almost consistently improve the final matching accuracy [36, 35, 23] as long as the network can fit into the GPU memory. However, up-sampling the input image to infinity causes issues because the information contained in the original image is fixed. Increasing the image size implies the receptive field of a deep neural network will reduce and so will the descriptiveness of the feature maps. Therefore, there must be an optimal resolution  $\mathbb{X}$  for a network to achieve its best performance for a given input. Thanks to the light-weight design of  $\mathbb{X}$ RCNet and the multi-GPU inference, we ran a series of experiments to confirm the existence of the optimal  $\mathbb{X}$  given a pre-trained  $\mathbb{X}$ RCNet by varying the up-sampling rate of the testing images.

Particularly, we resize the image of HPatches from 1280 pixels up to 4K ( $3840 \times 2160$ ) with fixed aspect ratio and evaluate. Fig. 6 shows the total area under the accuracy curve of MMA. We discover that the best matching accuracy increases with respect to the image resolution and gradually saturates around the resolution 3k. Using an image resolution higher than 3k reduces the matching accuracy. The accuracy at  $\mathbb{X}$ RCNet-3k surpassed the state-of-the-art DCN performance in the same error band on both HPatches (Fig. 4). For InLoc,  $\mathbb{X}$ RCNet-4k further surpassed  $\mathbb{X}$ RCNet-3k (See Tab. 4 and Fig. 5) possibly because of the relatively larger mean native resolution shown in Tab 2. Unfortunately, the  $\mathbb{X}$ RCNet-1.6k gives the best performance on Achen Day-Night which is inconsistent. However, we observe individual cases illustrated in Fig. 8, up-sampling remains effective as the heatmap of the  $\mathbb{X}$ RCNet-3k (right) is less ambiguous in the repetitive regions over  $\mathbb{X}$ RCNet-1.6k (left). The inconsistent results on Achen Day-Night is possibly due to the a much smaller number of testing pairs compared with other datasets (98 pairs in Achen Day-Night



Figure 8: **Left quadrant:** top row represents a heatmap from ResNet101, while the bottom row is from a light-weight ResNet18. The left column was produced from a model with NC filtering, while the right column has no NC filtering. Removing the NC reduces the capability of differentiating repetitive patterns such as the windows and therefore affects the matching accuracy. **Right:** the query night image with the chosen keypoint location marked with a red star and the heatmap produced from a ResNet18 model without NC filtering but using a high resolution image. It can be seen that the increased resolution balanced the issue of being sensitive to repetitive patterns without NC.

vs 108x5 pairs in HPatches and 329x10 pairs in InLoc).

### 4.3. Feature Backbone

In the end, we show experiments with different feature backbone architectures on HPatches. We have evaluated the matching accuracy using variant of both the ResNet and the HRNet backbones. In Fig. 7, it can be seen that when using the ResNet18 and ResNet50, the performance of the DualRC is almost identical to the original DualRC with ResNet101. The HRNet is another candidate we consider to replace the original feature backbone for the DualRC.

However, HRNet seems less competitive when integrated with the correspondence network. This is possibly because of the small number of channels in the lower layer and reduces the descriptiveness of the feature map for the lower layers. We also tested FPN with 128 and 256 channels. Although the 128 channel does not affect the accuracy much, the channel number is a relatively small cost to afford. We adopt 256 as default channel number.

## 5. Conclusion

In this paper, we propose the  $\mathbb{X}$ Resolution Correspondence Network, which is the result of a systematic study of the state-of-the-art dense correspondence networks. We noticed that a key component of these networks — the learned 4D correlation tensor — does not have a huge impact on the performance. Therefore, removing the 4D filtering with learnable parameters allows  $\mathbb{X}$ RCNet to learn quicker and enables it to process input images with resolution up to 4K. The proposed a DCN architecture outperforms state-of-the-art on HPatches and InLoc, and enables us to investigate the intriguing question if increasing the input image resolution is always beneficial to matching accuracy. Through extensive experimentation and a thorough ablation study we observe a saturation of the matching performance over the optimal resolution  $\mathbb{X}$ . We hope this work can shed light on how to design efficient and effective correspondence networks, while acting as a first step towards the interesting problem how the scale differences in input images affect DCNs.

**Acknowledgements** We would like to thank Umar Ahmed, Guy Newsom and the rest of the XYZ Reality team for helping out with various design concepts and fruitful discussions. In addition, we are grateful to Olivia Wiles for kindly providing the raw data for comparison.

## References

- [1] Vassileios Balntas, Karel Lenc, Andrea Vedaldi, and Krystian Mikolajczyk. Hpatches: A benchmark and evaluation of handcrafted and learned local descriptors. In *Proceedings of IEEE Intl. Conf. on Computer Vision and Pattern Recognition (CVPR)*, 2017. [2](#), [6](#)
- [2] Herbert Bay, Tinne Tuytelaars, and Luc Van Gool. Surf: Speeded up robust features. In *Proceedings of the European Conference on Computer Vision (ECCV)*, 2006. [1](#), [3](#)
- [3] Michael Calonder, Vincent Lepetit, Christoph Strecha, and Pascal Fua. BRIEF: Binary robust independent elementary features. In *Proceedings of the European Conference on Computer Vision (ECCV)*, pages 778–792, 2010. [3](#)
- [4] Ting Chen, Simon Kornblith, Mohammad Norouzi, and Geoffrey Hinton. A Simple Framework for Contrastive Learning of Visual Representations. *Preprint*, 2020. [2](#)
- [5] Bowen Cheng, Bin Xiao, Jingdong Wang, Honghui Shi, Thomas S. Huang, and Lei Zhang. HigherHRNet: Scale-Aware Representation Learning for Bottom-Up Human Pose Estimation. In *Proceedings of IEEE Intl. Conf. on Computer Vision and Pattern Recognition (CVPR)*, 2020. [6](#)
- [6] Christopher Choy, Junyoung Gwak, and Silvio Savarese. 4D spatio-temporal convnets: Minkowski convolutional neural networks. In *Proceedings of IEEE Intl. Conf. on Computer Vision and Pattern Recognition (CVPR)*, pages 3070–3079, 2019. [3](#), [5](#)
- [7] Christopher B Choy and Silvio Savarese. Universal Correspondence Network. In *Proceedings of Conf. on Neural Information Processing Systems (NeurIPS)*, pages 1–9, 2016. [2](#), [5](#)
- [8] Daniel DeTone, Tomasz Malisiewicz, and Andrew Rabenovich. Superpoint: Self-supervised interest point detection and description. In *Proceedings of IEEE Intl. Conf. on Computer Vision and Pattern Recognition (CVPR)*, 2018. [1](#), [7](#)
- [9] Mihai Dusmanu, Ignacio Rocco, Tomas Pajdla, Marc Pollefeys, Josef Sivic, Akihiko Torii, and Torsten Sattler. D2-net: A trainable cnn for joint detection and description of local features. In *Proceedings of IEEE Intl. Conf. on Computer Vision and Pattern Recognition (CVPR)*, 2019. [1](#), [3](#), [5](#), [6](#)
- [10] Dorian Galvez-Lopez and Juan D. Tardos. Bags of Binary Words for Fast Place Recognition in Image Sequences. *IEEE Trans. on Robotics (ToR)*, 28(5):1188–1197, 2012. [3](#)
- [11] Xiao-shan Gao, Xiao-rong Hou, Jianliang Tang, and Hangfei Cheng. Complete solution classification for the perspective-three-point problem. *IEEE Trans. Pattern Anal. Machine Intell. (PAMI)*, 25(8):930–943, 2003. [7](#)
- [12] Steffen Gauglitz, Tobias Höllerer, and Matthew Turk. Evaluation of interest point detectors and feature descriptors for visual tracking. *Intl. Journal of Computer Vision (IJCV)*, 2011. [1](#)
- [13] Hugo Germain, Guillaume Bourmaud, and Vincent Lepetit. S2DNet: Learning Accurate Correspondences for Sparse-to-Dense Feature Matching. In *Proceedings of the European Conference on Computer Vision (ECCV)*, 2020. [2](#), [5](#)
- [14] Kai Han, Rafael S. Rezende, Bumsub Ham, Kwan-Yee K. Wong, Minsu Cho, Cordelia Schmid, and Jean Ponce. Scnet: Learning semantic correspondence. In *Proceedings of Intl. Conf. on Computer Vision (ICCV)*, 2017. [3](#)
- [15] Kaiming He, Xiangyu Zhang, Shaoqing Ren, and Jian Sun. Deep residual learning for image recognition. In *Proceedings of IEEE Intl. Conf. on Computer Vision and Pattern Recognition (CVPR)*, 2016. [6](#)
- [16] Tong He, Zhi Zhang, Hang Zhang, Zhongyue Zhang, Junyuan Xie, Mu Li, and Amazon Web Services. Bag of Tricks for Image Classification with Convolutional Neural Networks. In *Proceedings of IEEE Intl. Conf. on Computer Vision and Pattern Recognition (CVPR)*, 2019. [2](#)
- [17] Shuaiyi Huang, Qiuyue Wang, Songyang Zhang, Shipeng Yan, and Xuming He. Dynamic context correspondence network for semantic alignment. In *Proceedings of Intl. Conf. on Computer Vision (ICCV)*, 2019. [3](#)
- [18] Diederik P. Kingma and Jimmy Lei Ba. Adam: a Method for Stochastic Optimization. In *Proceedings of Intl. Conf. on Learning Representations (ICLR)*, pages 1–15, 2015. [5](#)

[19] Junghyup Lee, Dohyung Kim, Jean Ponce, and Bumsub Ham. Sfnet: Learning object-aware semantic correspondence. In *Proceedings of IEEE Intl. Conf. on Computer Vision and Pattern Recognition (CVPR)*, 2019. 3

[20] Stefan Leutenegger, Margarita Chli, and Roland Y Siegwart. Brisk: Binary robust invariant scalable keypoints. In *Proceedings of Intl. Conf. on Computer Vision (ICCV)*, 2011. 1, 3

[21] Li-Jia Li, Kai Li, Fei Fei Li, Jia Deng, Wei Dong, Richard Socher, and Li Fei-Fei. ImageNet: a Large-Scale Hierarchical Image Database Shrimp Project View project hybrid intrusion detection systems View project ImageNet: A Large-Scale Hierarchical Image Database. In *Proceedings of IEEE Intl. Conf. on Computer Vision and Pattern Recognition (CVPR)*, 2009. 6

[22] Shuda Li, Kai Han, Theo W. Costain, Henry Howard-Jenkins, and Victor Prisacariu. Correspondence networks with adaptive neighbourhood consensus. In *Proceedings of IEEE Intl. Conf. on Computer Vision and Pattern Recognition (CVPR)*, 2020. 1, 3, 4, 5, 6

[23] Xinghui Li, Kai Han, Shuda Li, and Victor Adrian Prisacariu. Dual-Resolution Correspondence Networks. In *Proceedings of Conf. on Neural Information Processing Systems (NeurIPS)*, 2020. 1, 2, 3, 5, 6, 7, 8

[24] Zhengqi Li and Noah Snavely. Megadepth: Learning single-view depth prediction from internet photos. In *Proceedings of IEEE Intl. Conf. on Computer Vision and Pattern Recognition (CVPR)*, 2018. 5, 6

[25] Tsung-yi Lin, Piotr Doll, Ross Girshick, Kaiming He, Bharath Hariharan, Serge Belongie, and Facebook Ai. Feature pyramid networks for object detection. In *Proceedings of IEEE Intl. Conf. on Computer Vision and Pattern Recognition (CVPR)*, 2017. 6

[26] Ce Liu, Jenny Yuen, and Antonio Torralba. Sift flow: Dense correspondence across scenes and its applications. *IEEE Trans. Pattern Anal. Machine Intell. (PAMI)*, 2011. 1, 3

[27] David G Lowe. Distinctive image features from scale-invariant keypoints. *Intl. Journal of Computer Vision (IJCV)*, 2004. 1, 3

[28] Zixin Luo, Lei Zhou, Xuyang Bai, Hongkai Chen, Jiahui Zhang, Yao Yao, Shiwei Li, Tian Fang, and Long Quan. Aslfeat: Learning local features of accurate shape and localization. In *Proceedings of IEEE Intl. Conf. on Computer Vision and Pattern Recognition (CVPR)*, 2020. 1, 3

[29] Juhong Min, Jongmin Lee, Jean Ponce, and Minsu Cho. Hyperpixel flow: Semantic correspondence with multi-layer neural features. In *Proceedings of Intl. Conf. on Computer Vision (ICCV)*, 2019. 3

[30] Juhong Min, Jongmin Lee, Jean Ponce, and Minsu Cho. Learning to Compose Hypercolumns for Visual Correspondence. In *Proceedings of the European Conference on Computer Vision (ECCV)*, 2020. 3

[31] Hyeyoung Noh, Andre Araujo, Jack Sim, Tobias Weyand, and Bohyung Han. Large-Scale Image Retrieval with Attentive Deep Local Features. In *Proceedings of Intl. Conf. on Computer Vision (ICCV)*, pages 3476–3485, 2017. 2, 7

[32] Adam Paszke, Sam Gross, Francisco Massa, Adam Lerer, James Bradbury, Gregory Chanan, Trevor Killeen, Zeming Lin, Natalia Gimelshein, Luca Antiga, Alban Desmaison, Andreas Kopf, Edward Yang, Zachary DeVito, Martin Raison, Alykhan Tejani, Sasank Chilamkurthy, Benoit Steiner, Lu Fang, Junjie Bai, and Soumith Chintala. Pytorch: An imperative style, high-performance deep learning library. In *Proceedings of Conf. on Neural Information Processing Systems (NeurIPS)*, 2019. 6

[33] Francesco Pittaluga, Sanjeev J Koppal, Sing Bing Kang, and Sudipta N Sinha. Revealing Scenes by Inverting Structure from Motion Reconstructions. In *Proceedings of IEEE Intl. Conf. on Computer Vision and Pattern Recognition (CVPR)*, 2019. 3

[34] Jerome Revaud, Philippe Weinzaepfel, César De Souza, Noe Pion, Gabriela Csurka, Yohann Cabon, and Martin Humenberger. R2D2: Repeatable and Reliable Detector and Descriptor. In *Proceedings of Conf. on Neural Information Processing Systems (NeurIPS)*, 2019. 1, 3, 6

[35] Ignacio Rocco, Relja Arandjelović, and Josef Sivic. Efficient neighbourhood consensus networks via submanifold sparse convolutions. In *Proceedings of the European Conference on Computer Vision (ECCV)*, 2020. 2, 3, 4, 5, 6, 7, 8

[36] Ignacio Rocco, Mircea Cimpoi, Relja Arandjelović, Akihiko Torii, Tomas Pajdla, and Josef Sivic. Neighbourhood consensus networks. In *Proceedings of Conf. on Neural Information Processing Systems (NeurIPS)*, 2018. 2, 3, 4, 5, 6, 8

[37] Edward Rosten, Reid Porter, and Tom Drummond. Faster and better: a machine learning approach to corner detection. *IEEE Trans. Pattern Anal. Machine Intell. (PAMI)*, 2010. 1

[38] Paul-Edouard Sarlin, Daniel DeTone, Tomasz Malisiewicz, and Andrew Rabinovich. Superglue: Learning feature matching with graph neural networks. In *Proceedings of IEEE Intl. Conf. on Computer Vision and Pattern Recognition (CVPR)*, 2020. 1, 3, 7

[39] Torsten Sattler, Will Maddern, Carl Toft, Akihiko Torii, Lars Hammarstrand, Erik Stenborg, Daniel Safari, Masatoshi Okutomi, Marc Pollefeys, Josef Sivic, Fredrik Kahl, and Tomas Pajdla. Benchmarking 6DOF Outdoor Visual Localization in Changing Conditions. In *Conference on Computer Vision and Pattern Recognition (CVPR)*, 2018. 3, 6

[40] Torsten Sattler, Tobias Weyand, Bastian Leibe, and Leif Kobbelt. Image Retrieval for Image-Based Localization Revisited. In *British Machine Vision Conference (BMVC)*, 2012. 3, 6

[41] Johannes L. Schönberger and Jan-Michael Frahm. Structure-from-motion revisited. In *Proceedings of IEEE Intl. Conf. on Computer Vision and Pattern Recognition (CVPR)*, 2016. 1, 3, 6

[42] Johannes Lutz Schönberger, Hans Hardmeier, Torsten Sattler, and Marc Pollefeys. Comparative Evaluation of Hand-Crafted and Learned Local Features Comparative Evaluation of Hand-Crafted and Learned Local Features. In *Proceedings of IEEE Intl. Conf. on Computer Vision and Pattern Recognition (CVPR)*, 2017. 3

[43] Johannes Lutz Schönberger, Enliang Zheng, Marc Pollefeys, and Jan-Michael Frahm. Pixelwise view selection for unstructured multi-view stereo. In *Proceedings of the European Conference on Computer Vision (ECCV)*, 2016. 1, 3, 6

[44] Hajime Taira, Masatoshi Okutomi, Torsten Sattler, Mircea Cimpoi, Marc Pollefeys, Josef Sivic, Tomas Pajdla, and Akihiko Torii. InLoc: Indoor visual localization with dense matching and view synthesis. In *Proceedings of IEEE Intl. Conf. on Computer Vision and Pattern Recognition (CVPR)*, 2018. [2](#), [7](#)

[45] Yurun Tian, Bin Fan, and Fuchao Wu. L2-Net: Deep learning of discriminative patch descriptor in Euclidean space. In *Proceedings of IEEE Intl. Conf. on Computer Vision and Pattern Recognition (CVPR)*, pages 6128–6136, 2017. [3](#)

[46] Yurun Tian, Xin Yu, Bin Fan, Fuchao Wu, Huub Heijnen, and Vassileios Balntas. Sosnet: Second order similarity regularization for local descriptor learning. In *Proceedings of IEEE Intl. Conf. on Computer Vision and Pattern Recognition (CVPR)*, 2019. [1](#), [3](#)

[47] Jingdong Wang, Ke Sun, Tianheng Cheng, Borui Jiang, Chaorui Deng, Yang Zhao, Dong Liu, Yadong Mu, Mingkui Tan, Xinggang Wang, Wenyu Liu, and Bin Xiao. Deep High-Resolution Representation Learning for Visual Recognition. *IEEE Trans. Pattern Anal. Machine Intell. (PAMI)*, 8828, 2020. [6](#)

[48] Jamie Watson, Oisin Mac Aodha, Daniyar Turmukhambetov, Gabriel J Brostow, and Michael Firman. Learning Stereo from Single Images. In *Proceedings of the European Conference on Computer Vision (ECCV)*, 2020. [3](#)

[49] Olivia Wiles, Sebastien Ehrhardt, and Andrew Zisserman. D2D: Learning to find good correspondences for image matching and manipulation. In *Proceedings of IEEE Intl. Conf. on Computer Vision and Pattern Recognition (CVPR)*, 2021. [1](#), [2](#), [3](#), [5](#)

[50] Nan Yang, Lukas von Stumberg, Rui Wang, and Daniel Cremers. D3VO: Deep Depth, Deep Pose and Deep Uncertainty for Monocular Visual Odometry. In *Proceedings of IEEE Intl. Conf. on Computer Vision and Pattern Recognition (CVPR)*, 2020. [3](#)

[51] Tsun-Yi Yang, Duy-Kien Nguyen, Huub Heijnen, and Vassileios Balntas. UR2KiD: Unifying Retrieval, Keypoint Detection, and Keypoint Description without Local Correspondence Supervision. In *Proceedings of IEEE Intl. Conf. on Computer Vision and Pattern Recognition (CVPR)*, 2020. [1](#)

[52] Kwang Moo Yi, Eduard Trulls, Yuki Ono, Vincent Lepetit, Mathieu Salzmann, and Pascal Fua. Learning to Find Good Correspondences. In *Proceedings of IEEE Intl. Conf. on Computer Vision and Pattern Recognition (CVPR)*, pages 2666–2674, 2018. [3](#)

[53] Andrei Zanfir and Cristian Sminchisescu. Deep Learning of Graph Matching. In *Proceedings of IEEE Intl. Conf. on Computer Vision and Pattern Recognition (CVPR)*, pages 2684–2693, 2018. [2](#)

[54] Jiahui Zhang, Dawei Sun, Zixin Luo, Anbang Yao, Lei Zhou, Tianwei Shen, Yurong Chen, Hongen Liao, and Long Quan. Learning two-view correspondences and geometry using order-aware network. In *Proceedings of Intl. Conf. on Computer Vision (ICCV)*, 2019. [1](#), [3](#)

[55] Zichao Zhang, Torsten Sattler, and Davide Scaramuzza. Reference Pose Generation for Visual Localization via Learned Features and View Synthesis. *Intl. Journal of Computer Vision (IJCV)*, 2020. [1](#)

# XXResolution Correspondence Networks

## -Supplementary Material-

This supplementary material provides extra details which are not presented in the main paper due to space limitations. In the following document we discuss the effects of using various re-sampling resolutions during testing in Sec. 1. In Sec. 2, we provide more in depth comparison on HPatches and propose a novel evaluation criterion to demonstrate the effectiveness of the XRCNet. In Sec. 3, we show more qualitative results on InLoc and Aachen Day-Night dataset, which further demonstrate the quality of the proposed model. Moreover, in Sec. 4 we demonstrate the accuracy of our XRCNet in the challenging task of 3D reconstruction using the Aachen Day-Night dataset. We conclude with a brief description of the source code released in Sec. 5.

First of all, we visualise the output feature maps and correlation maps of the key modules in XRCNet in Fig 1 to illustrate the effectiveness of the key modules when solving a correspondence task. We plot 5 examples of various training and testing images. Each is superimposed with the colour map representing the output feature maps or correlation maps of the corresponding modules. From left to right, we plot the coarse features maps from the FPN decoder, the fine feature maps, the 2D coarse correlation map calculated by querying the key point in the source image into the 4D correlation tensor, the same coarse correlation map querying into the 4D tensor after the first mutual matching layer and after the second mutual matching layer respectively. In the end, we plot the final 2D coarse correlation map and the fine correlation map after the re-weighting. For feature maps, we simply visualise the max values alone the channels. It can be noticed that the coarse and fine feature map contains similar patterns except the resolution difference possibly due to the original design of FPN layers. The raw 4D correlation tensor does show a peak around the ground truth point location but also contains significant amount of noise. After two rounds of mutual matching filtering, most of the noise are suppressed except a few ambiguous candidates, and the final re-weighting allows the network to look into the local area in detail so that XRCNet can make correct predictions in the end.

### 1. Effects of Different Re-sampling Resolutions

In this section we present both qualitative and quantitative analysis on HPatches when re-sampling the testing images into various resolutions. As shown in Fig. 2, we varied the input image resolution from 720 to 3840 (4K) with a step size of about 200. From left to right, we show the Mean Matching Accuracy (MMA) [1, 2] plots for the cases of illumination challenges, viewpoint challenges, and overall. The native resolution of the HPatches dataset is reported in Tab. 2 of the main paper.

We observe that the low re-sampling resolution has a major impact on the accuracy in the viewpoint challenges. In contrast, for illumination challenges, low resolution performs relatively well for the low error band ( $< 3$  pixels). However, the increased re-sampling resolution leads to better performance on the illumination challenge at the cost of a small decrease at the low error band. This is possibly due to stronger ambiguity in the local region in illumination scenarios. For example, the lighting changes introduce blur around many key points when transitioning from day to night. As the resolution increases, the predicted key point locations are more likely to converge towards more repeatable but less accurate areas. As far as the large error band is concerned, the performance of our method saturates for the illumination scenario while increasing for the viewpoint challenges as the re-sampling resolution increases. The area under the MMA curve is also provided to measure the overall accuracy. It can be seen that the performance gain using higher re-sampling resolution saturated around 2600 to 3400 with the peak performance at resolution 3000. Note that Fig. 8 in the main paper provides a clear visualisation of the overall performance and Fig 2 provides individual plots for each tested resolution.

We have also evaluated different re-sampling resolutions on the InLoc [5] dataset in Fig. 3. It can be seen that high-resolution images result in better relocalisation accuracy in terms of the translation error.

Fig. 4 shows the heatmaps of predicted target point using input images of various resolutions. The ground truth match is marked with a white dot. It can be seen that higher re-sampling resolutions consistently reduce the uncertainty indicated by

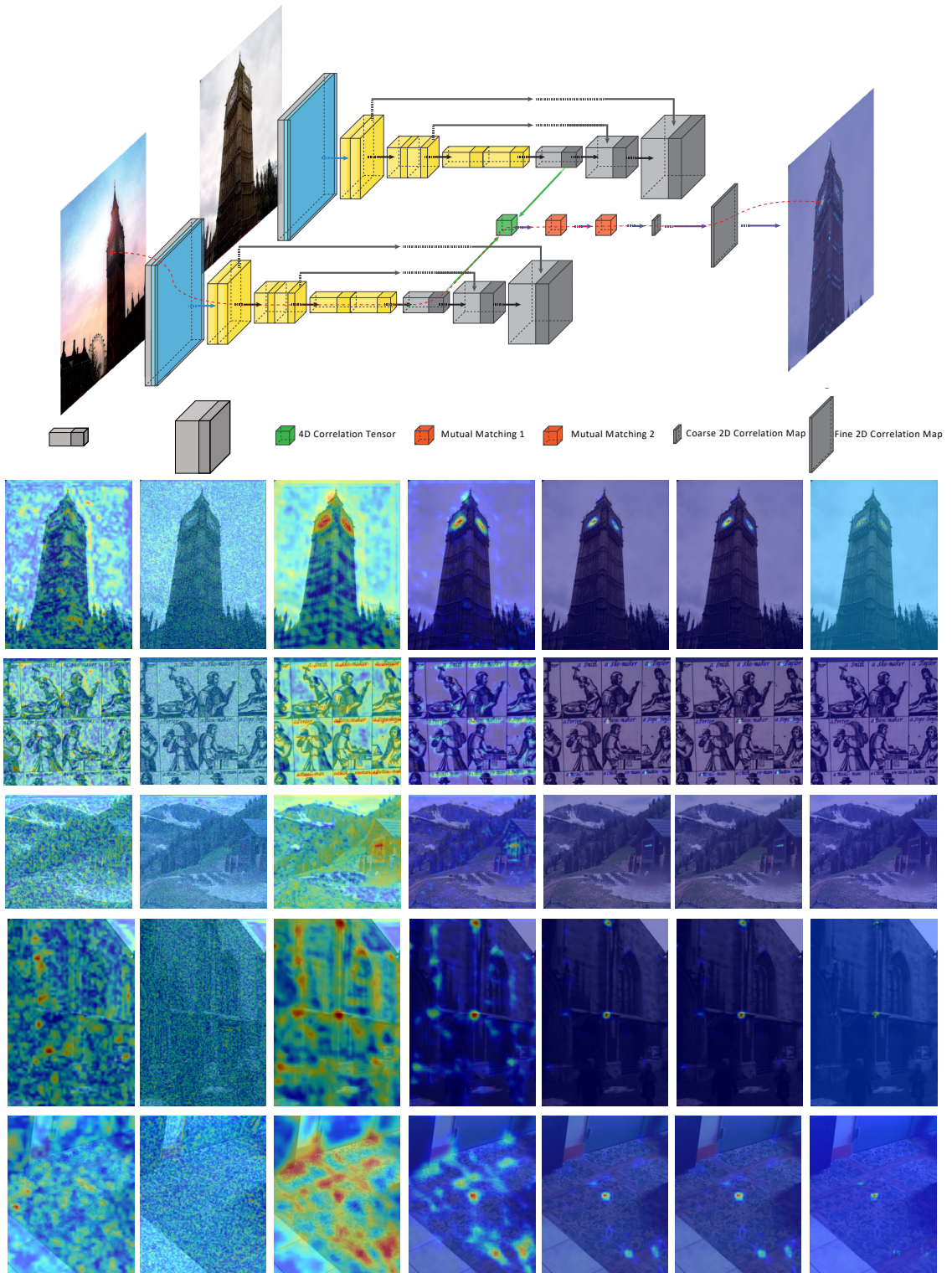


Figure 1: Visualisation of the feature maps and correlation maps of key components in XRCNet.

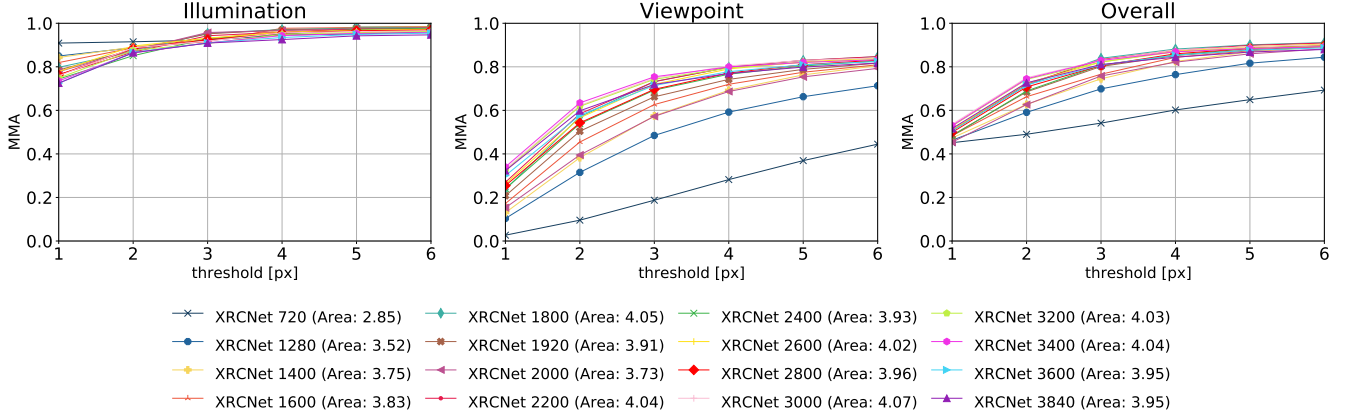


Figure 2: Comparison of XRCNet with respect to the up-sampled input image resolution evaluated on the HPatches dataset.

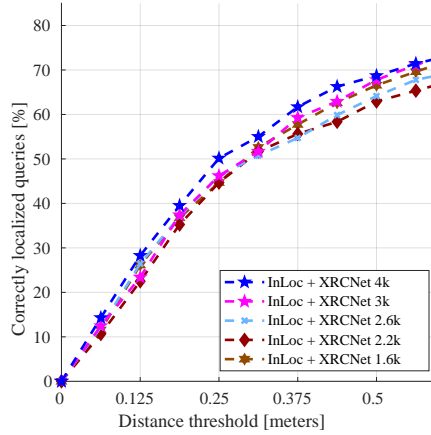


Figure 3: Comparison of XRCNet with respect to the up-sampled input image resolution on the InLoc dataset after geometric verification.

the size of the coloured blob. However, as the resolution further increases over 3000, the prediction becomes over-confident towards a close but inaccurate location. This is possibly because of the reduced receptive field of the feature backbone relative to the original image.

In addition to evaluating the re-sampling impact for inference, we also trained our correspondence network using various training image resolutions. Surprisingly, increasing the input resolution during training does not improve performance, as shown in Fig. 5. We hypothesise this is because various training image resolutions contain a fixed amount of information that a correspondence network can use. Therefore, we choose to use 400 px resolution during training in order to achieve a fair comparison with other baseline methods. Please note that all methods are trained with a batch size of 16 to accommodate higher resolution in the feature maps.

## 2. Qualitative Analysis — HPatches

In Fig. 6 and 7, we select six individual testing pairs to demonstrate that XRCNet outperforms DualRCNet [2] and SparseNC [3] respectively in terms of the ratio of correct matching predictions of top 2000 outputs<sup>1</sup>. It can be seen that XRCNet is capable of producing more reliable results than previous works. In this section we propose a novel evaluation criterion in supplement to the main results along with the qualitative comparison of Fig. 6. This new evaluation criterion can be formulated as:

<sup>1</sup>2000 is a arbitrary number. Following previous works of D2Net, DualRCNet and SparseNC, we also adopt 2000 for a fair comparison.

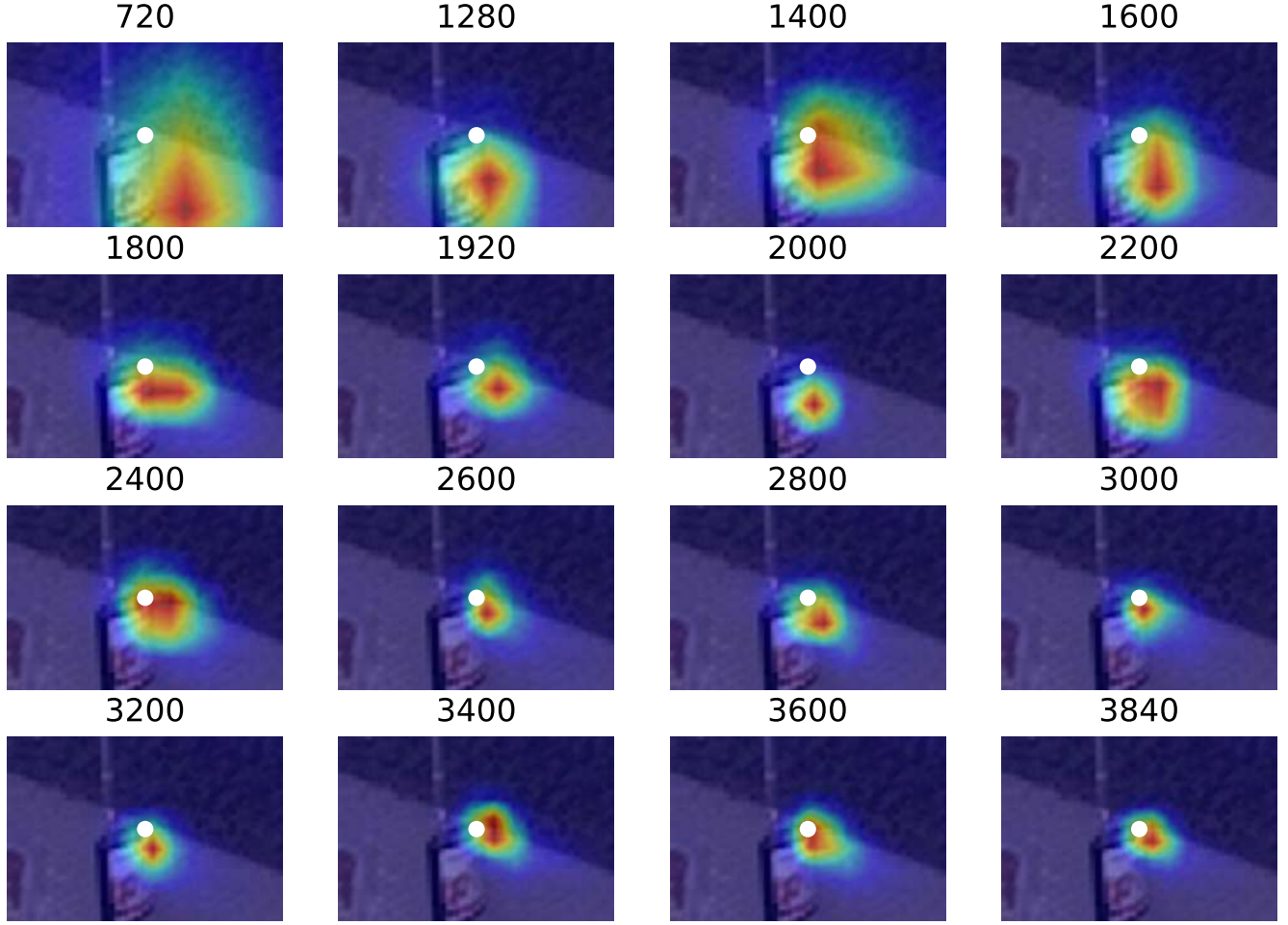


Figure 4: Produced keypoint heatmap from the correlation tensor overlayed at a reference image. The ground truth location of the query keypoint is denoted in white.

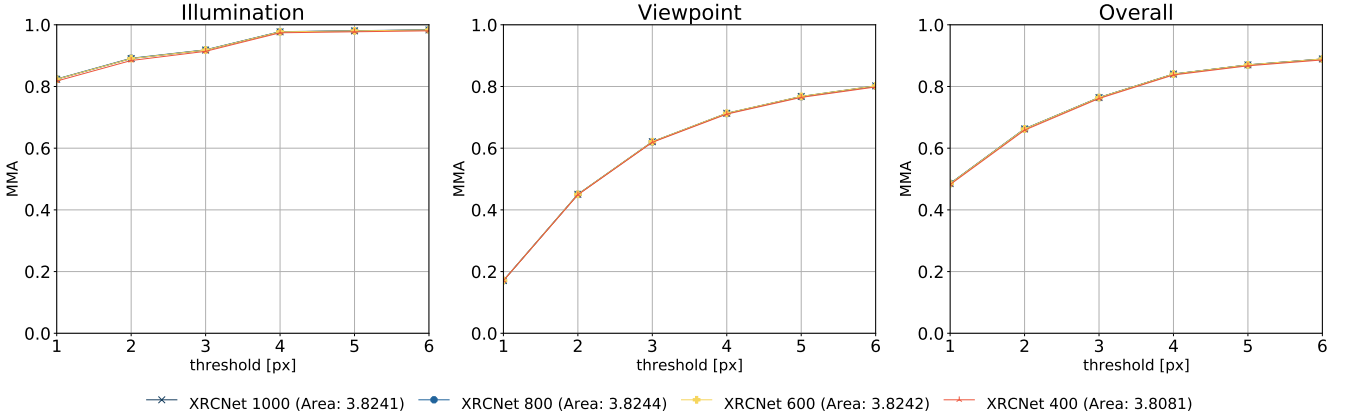


Figure 5: Training XRCNet with re-sampled image resolution of 400px to 1,000 px at every 200px.

$$\mathbb{N}(\tau^-; \tau^+, +, -) = \sum_i^N \mathbf{1}(c_i^+ > \tau^+ \cap c_i^- < \tau^-), \quad (1)$$

where  $c_i^+$  and  $c_i^-$  is the ratio of the correct matches out of all the predicted matches of two comparing methods denoted as '+' and '−', respectively.  $\tau^+$  and  $\tau^-$  are thresholds of the corresponding ratio.  $i \in \{1, 2, \dots, N\}$  is the index of the testing pairs in the dataset.  $\mathbf{1}(\cdot)$  is a binary indicator function such that  $\mathbf{1}(\text{True}) = 1$  and  $\mathbf{1}(\text{False}) = 0$ . As long as there exists the pixel-wise ground truth label, we can always adopt Equation 1 to calculate the number of pairs that favour the '+' method against the '−' method.

Equation 1 measures the number of testing image pairs that favours method + with respect to ratio  $\tau^-$  at a specific positive  $\tau^+$ . In other words,  $\mathbb{N}(\cdot)$  is a histogram of the testing pairs where the first method + achieves accuracy higher than the threshold  $\tau^+$  but the second method − achieves accuracy lower than  $\tau^-$ . In the top row of Fig 8, we illustrate plotting both the  $\mathbb{N}(\tau^-; \tau^+, \mathbb{X}\text{RCNet}, \text{DualRCNet})$  the blue curve vs  $\mathbb{N}(\tau^-; \tau^+, \text{DualRCNet}, \mathbb{X}\text{RCNet})$  the red curve over the range of  $\tau^- \in [0, \tau^+]$  with a step size of 0.1, and  $\tau^+$  is set to 0.75, 0.85 and 0.95, respectively. Similarly, in the bottom row of Fig. 8 we present both  $\mathbb{N}(\tau^-; \tau^+, \mathbb{X}\text{RCNet}, \text{SparseNC})$  as the blue curve vs  $\mathbb{N}(\tau^-; \tau^+, \text{SparseNC}, \mathbb{X}\text{RCNet})$  as the red curve. The three sub-figures in Fig. 8 compare the number of testing data that favours  $\mathbb{X}\text{RCNet}$  against those favouring DualRCNet/SparseNC. It demonstrates that the proposed  $\mathbb{X}\text{RCNet}$  consistently outperforms DualRCNet and SparseNC for all combination of  $\tau^-$  and  $\tau^+$  values as the number favouring  $\mathbb{X}\text{RCNet}$  is significantly higher than the number favouring DualRCNet/SparseNC.

### 3. Qualitative Analysis – InLoc and Aachen Day-Night

Fig. 9 illustrates the performance of  $\mathbb{X}\text{RCNet}$  on the InLoc dataset. Similarly to HPatches, the increase in resolution from 1600 to 3840 (4K) results in better performance. The 4K upsampling resolution for InLoc dataset performs better in terms of relocalisation accuracy than the rest. As mentioned in the main article, we hypothesise this due to the native resolution of testing images in InLoc is much higher than that of HPatches.

Fig. 10 shows visual examples of the proposed model evaluated on the Aachen Day-Night dataset [4].

### 4. 3D Reconstruction Using Dense Correspondences

To demonstrate a potential application of using the correspondence network, we plot the 3D point cloud reconstructed using the  $\mathbb{X}\text{RCNet}$  in Fig. 11 on the Aachen Day-Night reference images. We also compare the quality of the 3D reconstruction using  $\mathbb{X}\text{RCNet}$  and DualRCNet in Fig. 12. It can be seen that the quality of the reconstructed models are fairly close for the two methods.

### 5. Code

We include code as part of the supplementary material to allow for reproducibility of the results as well as retraining the models. Our code is made publicly available here: <https://xyz-r-d.github.io/xrcnet>.

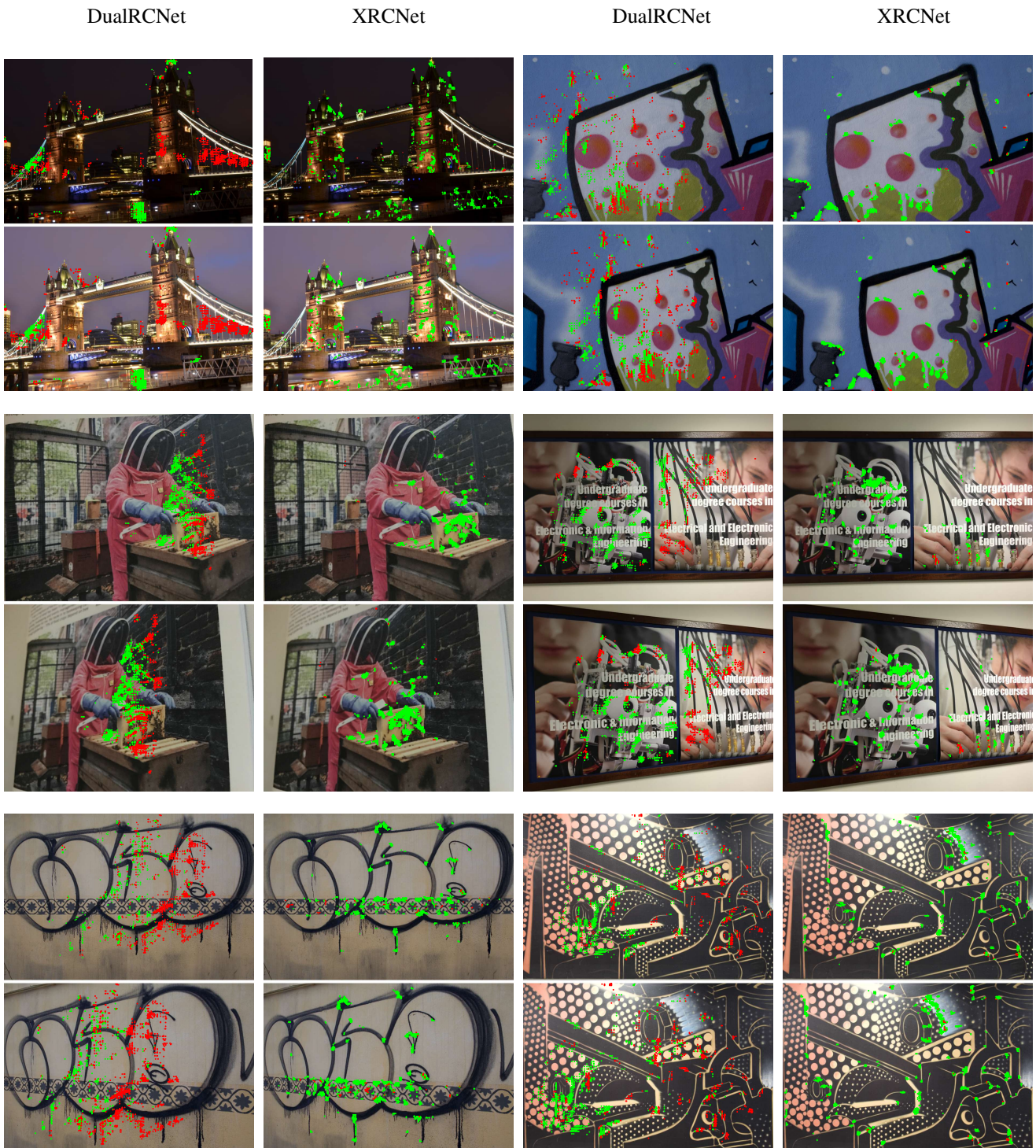


Figure 6: Qualitative comparison between XRCNet and DualRCNet on HPatches. The green dots represent the correct matches whose errors are within 3 pixels, and red dots the incorrect matches. XRCNet produces more correct matches out of the top 2000 matches than DualRCNet.

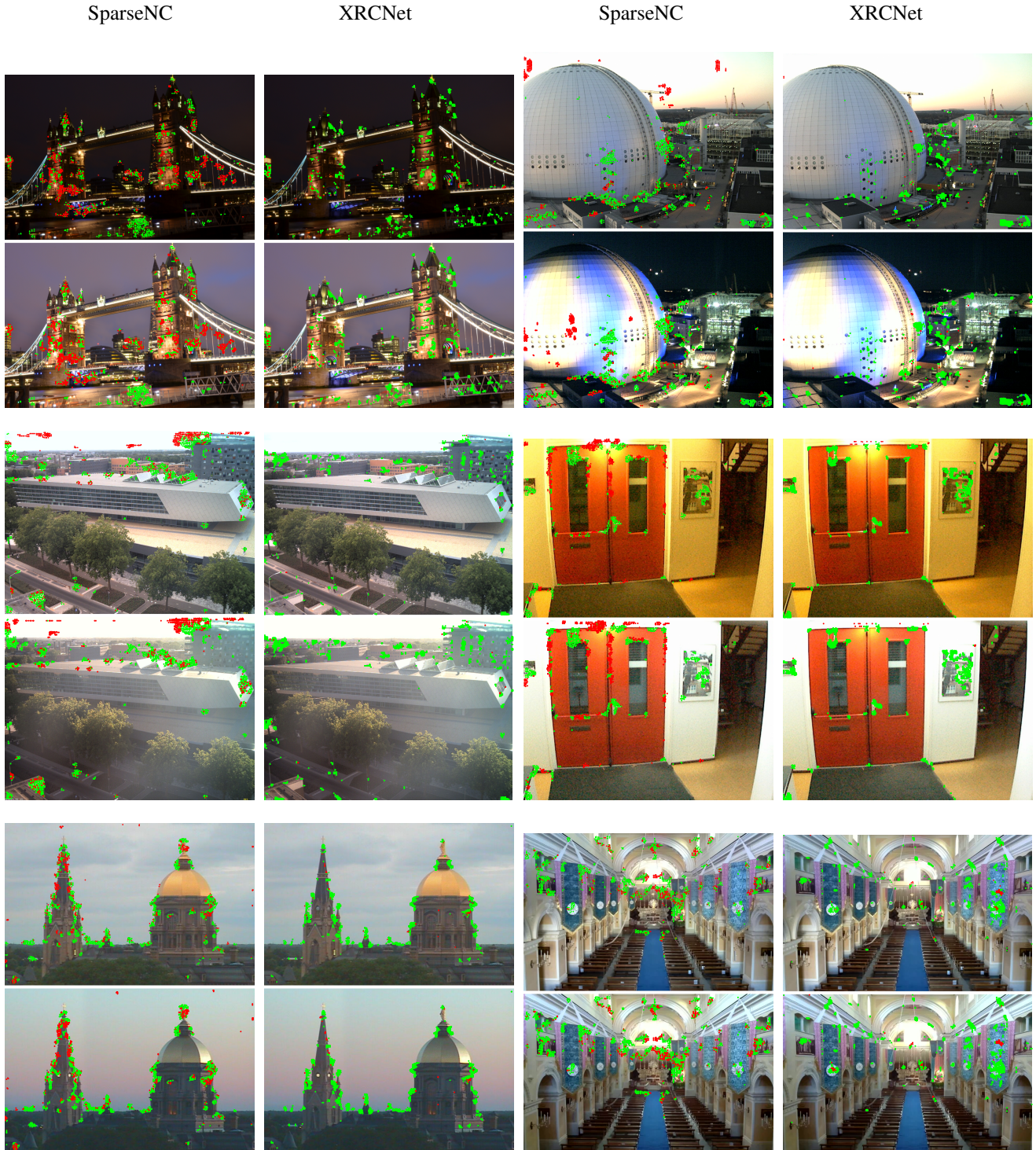


Figure 7: Qualitative comparison between XRCNet and SparseNC on HPatches. The green dots represent the correct matches whose errors are within 3 pixels, and red dots the incorrect matches. XRCNet produces more correct matches out of the top 2000 matches than SparseNC.

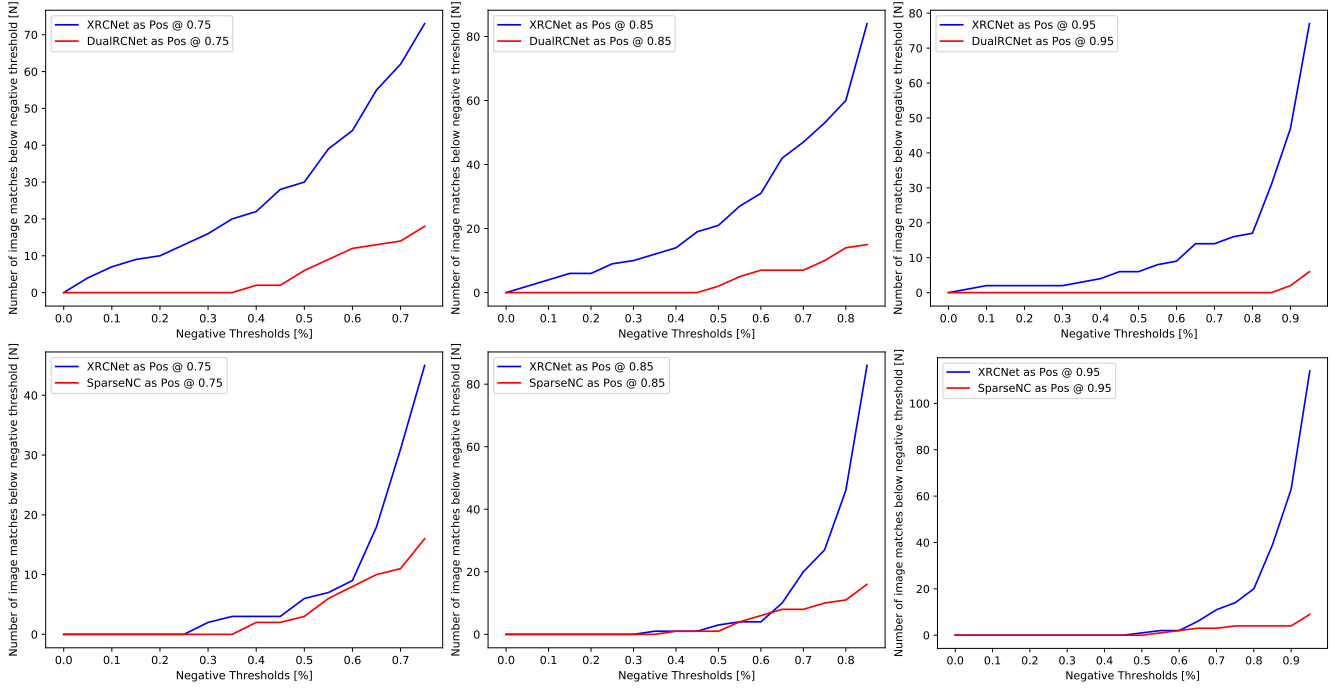


Figure 8: **Top row:** The comparison of the number of testing pairs that XRCNet outperforms DualRCNet (blue curve) and DualRCNet outperforms XRCNet using Equation 1. **Bottom row:** Similar comparison between XRCNet and SparseNC. For all comparisons, the  $\tau^+$  is chosen as 75%, 85%, and 95% for both curves.  $\tau^-$  in Equation 1 is denoted as the Negative Threshold. 'Pos' denotes '+' method and 0.75 represent the  $\tau^+$  ratio threshold.

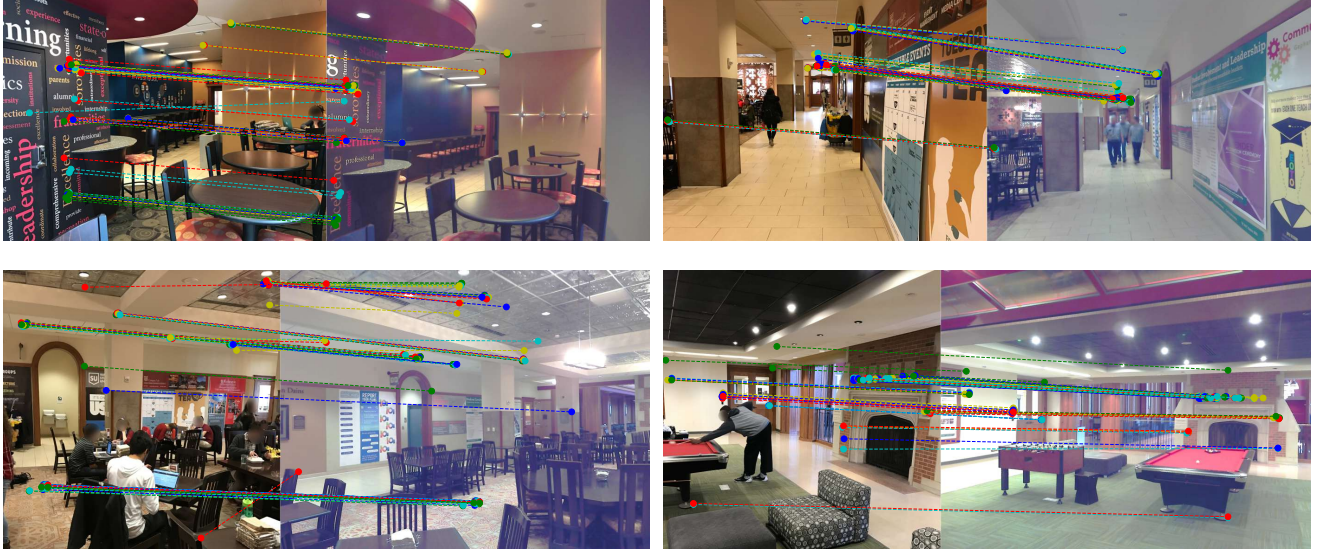


Figure 9: Examples of XRCNet running on the Aachen Day-Night dataset - top 2000 matches are displayed. It is worth pointing out the output matches with high reliability scores are heavily clustered in relatively small regions and may overlap each other.

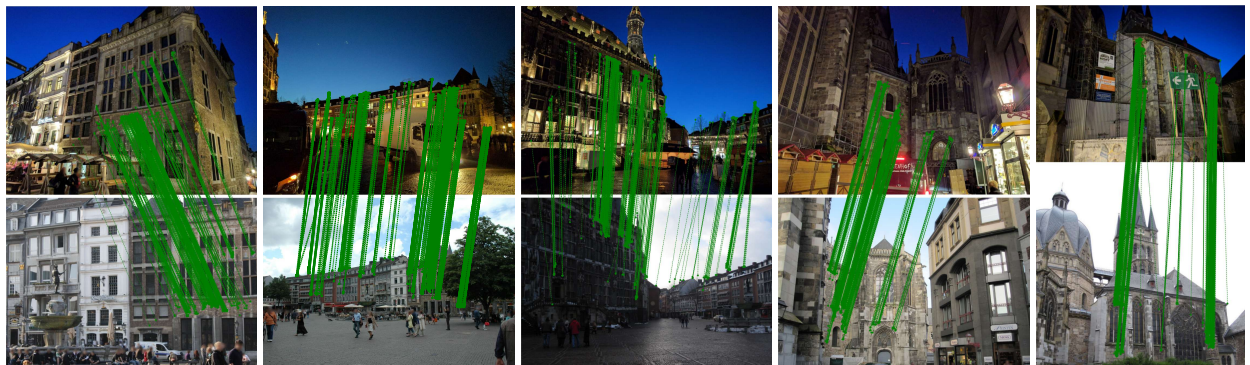


Figure 10: Examples of XRCNet running on the Aachen Day-Night dataset - top 2000 matches are displayed. It is worth pointing out the output matches with high reliability scores are heavily clustered in relatively small regions and may overlap each other.



Figure 11: 3D model reconstructed using correspondences obtained by  $\mathbb{X}$ RCNet for the Aachen Day-Night dataset.



Figure 12: Qualitative comparison of XRCNet (top) and DualRCNet (bottom) 3D model reconstructions on the Aachen Day-Night dataset.

## References

- [1] Vassileios Balntas, Karel Lenc, Andrea Vedaldi, and Krystian Mikolajczyk. Hpatches: A benchmark and evaluation of handcrafted and learned local descriptors. In *Proceedings of IEEE Intl. Conf. on Computer Vision and Pattern Recognition (CVPR)*, 2017. [1](#)
- [2] Xinghui Li, Kai Han, Shuda Li, and Victor Adrian Prisacariu. Dual-Resolution Correspondence Networks. In *Proceedings of Conf. on Neural Information Processing Systems (NeurIPS)*, 2020. [1, 3](#)
- [3] Ignacio Rocco, Relja Arandjelović, and Josef Sivic. Efficient neighbourhood consensus networks via submanifold sparse convolutions. In *Proceedings of the European Conference on Computer Vision (ECCV)*, 2020. [3](#)
- [4] Torsten Sattler, Akihiko Torii, Josef Sivic, Marc Pollefeys, Hajime Taira, Masatoshi Okutomi, and Tomas Pajdla. Are large-scale 3d models really necessary for accurate visual localization? In *Proceedings of IEEE Intl. Conf. on Computer Vision and Pattern Recognition (CVPR)*, 2017. [5](#)
- [5] Hajime Taira, Masatoshi Okutomi, Torsten Sattler, Mircea Cimpoi, Marc Pollefeys, Josef Sivic, Tomas Pajdla, and Akihiko Torii. InLoc: Indoor visual localization with dense matching and view synthesis. In *Proceedings of IEEE Intl. Conf. on Computer Vision and Pattern Recognition (CVPR)*, 2018. [1](#)